Fast Convergent Schrödinger-Poisson Solver for the Static and Dynamic Analysis of Carbon Nanotube Field Effect Transistors

Mahdi Pourfath and Hans Kosina

Institute for Microelectronics, Technische Universität Wien,
Gußhausstraße 27–29, A-1040 Wien, Austria
pourfath@iue.tuwien.ac.at

Abstract. Carbon nanotube field-effect transistors have been studied in recent years as a potential alternative to CMOS devices, because of the capability of ballistic transport. In order to account for the ballistic transport we solved the coupled Poisson and Schrödinger equations for the analysis of these devices. Conventionally the coupled Schrödinger-Poisson equation is solved iteratively with appropriate numerical damping. Often convergence problems occur. In this work we show that this problem is due to inappropriate energy discretization, and by using an adaptive integration method the simulation time is reduced and most of the simulations converge in a few iterations. Based on this approach we investigated the static and dynamic behavior of carbon nanotube field effect transistors.

1 Introduction

Exceptional electronic and mechanical properties together with nanoscale diameter make carbon nanotubes (CNTs) a candidate for nanoscale field effect transistors (FETs). While early devices have shown poor device characteristics, high performance devices were achieved recently [17, 11, 5, 7, 14]. In short devices (less than 100 nm) carrier transport through the device is nearly ballistic [5, 6]. As described in the next section the coupled Poisson and Schrödinger equation system was solved to study the static response of CNTFETs. We show that by using an adaptive integration method for calculating carrier concentration and current density, simulations converge very fast while the results are very accurate. Based on the Quasi Static Approximation (QSA) the dynamic response of these devices is also investigated.

The contact between metal and CNT can be of Ohmic [6] or Schottky type [1]. In this work we focus on Ohmic contact CNTFETs which theoretically [4] and experimentally [5] show better performance than Schottky contact devices. In a p-type device with ohmic contacts holes see no barrier while the barrier height for electrons is E_g. By changing the gate voltage the transmission coefficient of holes through the device is modulated and as a result the total current changes [6].

I. Lirkov, S. Margenov, and J. Waśniewski (Eds.): LSSC 2005, LNCS 3743, pp. 578–585, 2006.
© Springer-Verlag Berlin Heidelberg 2006

2 Approach

In this section the models which were used to study the static and dynamic response of CNTFETs are explained. As it will be shown in the next section a good agreement between simulation and experimental results is achieved.

2.1 Static Response

In order to account for the ballistic transport we solved the coupled Poisson and Schrödinger equations for CNTFETs.

$$\frac{\partial^2 V}{\partial \rho^2} + \frac{1}{\rho}\frac{\partial V}{\partial \rho} + \frac{\partial^2 V}{\partial z^2} = -\frac{Q}{\epsilon} \tag{1}$$

$$-\frac{\hbar^2}{2\mathrm{m}^*}\frac{\partial^2 \Psi_{s,d}^{n,p}}{\partial z^2} + (U^{n,p} - E)\Psi_{s,d}^{n,p} = 0 \tag{2}$$

We considered an azimuthal symmetric structure, in which the gate surrounds the CNT, such that the Poisson equation (1) is restricted to two-dimensions. In (1) $V(\rho, z)$ is the electrostatic potential, and Q is the space charge density.

In the Schrödinger equation (2) the effective mass is assumed to be $\mathrm{m}^* = 0.05\mathrm{m}_0$ for both electrons and holes [19]. In (2) superscripts denote the type of the carriers. Subscripts denote the contacts, where s stands for the source contact and d for the drain contact. For example, Ψ_s^n is the wave function associated with electrons that have been injected from the source contact, and U^n is the potential energy that is seen by electrons. The Schrödinger equation is just solved on the surface of the tube, and is restricted to one-dimension because of azimuthal symmetry.

The space charge density in (1) is calculated as:

$$Q = \frac{\mathrm{q}(p - n)\delta(\rho - \rho_{cnt})}{2\pi\rho} \tag{3}$$

where q is the electron charge, and n and p are total electron and hole concentrations per unit length. In (3) δ/ρ is the Dirac delta function in cylindrical coordinates, implying that carriers were taken into account by means of a sheet charge distributed uniformly over the surface of the CNT [8].

Including the source and drain injection components, the total electron concentration in the CNT is calculated as:

$$\begin{aligned} n &= \frac{4}{2\pi}\int f_s|\Psi_s^n|^2 dk_s + \frac{4}{2\pi}\int f_d|\Psi_d^n|^2 dk_d \\ &= \int \frac{\sqrt{2\mathrm{m}^*}}{\pi\hbar\sqrt{E_s}} f_s|\Psi_s|^2 dE_s + \int \frac{\sqrt{2\mathrm{m}^*}}{\pi\hbar\sqrt{E_d}} f_d|\Psi_d|^2 dE_d \end{aligned} \tag{4}$$

where $f_{s,d}$ are equilibrium Fermi functions at the source and drain contacts. All our calculations assume a CNT with 0.5 eV band gap [5]. The total hole concentration in the CNT is calculated analogously.

The Landauer-Büttiker formula [3] is used for calculating the current:

$$I^{n,p} = \frac{4\mathrm{q}}{\mathrm{h}} \int [f_s^{n,p}(E) - f_d^{n,p}(E)] T_c^{n,p}(E) dE \tag{5}$$

where $T_c^{n,p}(E)$ are the transmission coefficients of electrons and holes, respectively, through the device. The factor 4 in (4) and (5) stems from the twofold band and twofold spin degeneracy.

Conventionally the coupled Schrödinger and Poisson equations are solved iteratively [20], by using an appropriate numerical damping factor α. At the $(k+1)^{\mathrm{th}}$ iteration the Schrödinger equation is solved using the electrostatic potential V^k from the last iteration and the new space charge density Q^{k+1} is calculated. The Poisson equation is then solved by using Q^{k+1} and an intermediate new electrostatic potential is calculated V_{int}^{k+1}. Finally V^{k+1} is calculated as:

$$V^{k+1} = \alpha V_{\mathrm{int}}^{k+1} + (1-\alpha) V^k \tag{6}$$

where $0 < \alpha < 1$. Successive iteration continues until a convergence criterion is satisfied. In this work an adaptive damping factor was used [10]. The damping factor is initially set to $\alpha = 1$. If the potential update $|V^{k+1} - V^k|$ increases from one iteration to the next iteration or remains constant the damping factor decreases by a constant factor. We used $\alpha = \alpha \times 0.8$ as suggested by [10]. If a high damping factor is initially selected the simulations may oscillate and will not converge. Using a low damping factor will result in long simulation time. We show that by appropriate evaluation of the carrier concentration this problem can be avoided. The integration in (4) and (5) are calculated in an energy interval $[E_{\mathrm{min}}, E_{\mathrm{max}}]$. In the simplest way the interval is divided into equidistant steps. By using this method narrow resonances at some energies may be missed or may not be evaluated correctly. In successive iterations as the potential profile changes the position of the resonances will also change, and it is possible that a resonance point locates very near to one of the energy steps. In this case the carrier concentration suddenly changes and as a result the simulation would oscillate and not converge. To avoid this problem the accuracy of the integration should be independent of the location of resonances. By using an adaptive integration method the integrations in (4) and (5) can be evaluated with a desirable accuracy. Assume f is an integrable function, and $[a, b]$ is the interval of integration. To compute

$$I = \int_a^b f(x) dx \tag{7}$$

adaptively I is calculated with two different integration methods, I_1 and I_2. If the relative difference of the two approximations is less than a predefined tolerance the integration is accepted, otherwise the interval [a,b] is divided into two equal parts $[a, c]$ and $[c, b]$, where $c = (a+b)/2$, and the two respective integrals are computed independently.

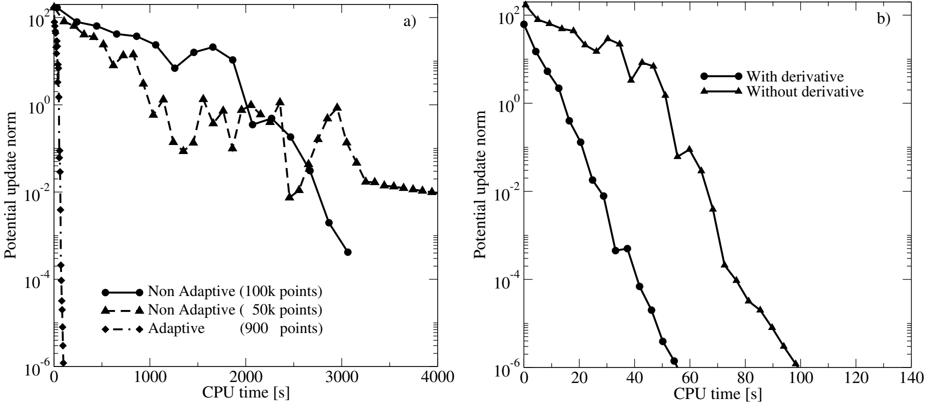

Fig. 1. The comparison of CPU time demand on an IBM-RS6000 for the same iterative simulation, but with different integration methods. The norm of the potential update is considered as a measure of convergence. a) Shows the results for adaptive and non adaptive integration. b) Show the result for adaptive integration with and without the derivative of carrier concentration with respect to the electrostatic potential.

$$I = \int_a^c f(x)dx + \int_c^b f(x)dx \tag{8}$$

The same procedure is performed for each of these integrals. The advantage of this methods is that the steps are non-equidistant, so there are many points around the resonances while in other regions there are few points. In this work an adaptive Simpson quadrature [15] is used. In this method the two successive Simpson approximates are calculated:

$$I_1 = \frac{h}{6}(f(a) + 4f(c) + f(b)) \tag{9}$$

$$I_2 = \frac{h}{12}(f(a) + 4f(d) + 2f(c) + 4f(e) + f(b)) \tag{10}$$

where $d = (a+c)/2$, and $e = (c+b)/2$. If $|I_1 - I_2| \leq \mathrm{tol} \times |I_2|$ the integration is evaluated within one step of Romberg extrapolation: $I = I_2 + (I_2 - I_1)/15$. Fig. 1-a shows the CPU time demand on an IBM-RS6000 for the same iterative simulation using adaptive integration and non-adaptive integration with 5×10^4 and 10^5 points. Increasing the number of data points in the non adaptive method the simulation becomes more stable. Using adaptive integration method, only 9×10^2 points are required and most of the simulations can start with a high damping factor ($\alpha = 1$) and no or few oscillations occur. Therefore a high damping factor is used for all the iterations and as a result simulations converge very fast. It is also possible to make the simulations more stable by providing the derivate of carrier concentration with respect to the electrostatic potential for the Poisson solver [12, 2]. In general there is no exact form for this term, but $\partial n/\partial \phi \approx \mathrm{q}\, \partial n/\partial E_F$ can be considered as a good

approximation [12]. As shown in Fig. 1-b by including the derivate of carrier concentration with respect to the electrostatic potential, the stability of simulations increases and the simulation time decreases.

2.2 Dynamic Response

To study the dynamic behavior of CNTFETs, the QSA was used. Generally in this method device capacitances are given by the derivatives of the various charges with respect to the terminal voltages:

$$C_{ij} = \chi_{ij} \left. \frac{\partial Q_i}{\partial V_j} \right|_{V_{k \neq j}=0} \tag{11}$$

where the indices i, j, k represent terminals (gate, source or drain), and $\chi_{ij} = -1$ for $i \neq j$ and $\chi_{ij} = +1$ for $i = j$. The differentiation of these expressions is performed numerically over steady state charges [18]. This method is widely used for the analysis of conventional semiconductor devices, where the charge in the semiconductor device is partitioned into two parts indicating the contribution of the source and drain contacts [18, 13]. For example, the gate-source capacitance is calculated by

$$C_{sg} = \frac{\partial Q_{se}}{\partial V_{gs}} + \frac{\partial Q_{st}}{\partial V_{gs}} = C_{se} + C_{sq} \tag{12}$$

where Q_{se} is total charge on the source contact and Q_{st} is the total charge on the tube injected from the source contact. As shown in (12) the total gate-source capacitance is split into two components, the first term indicates the electrostatic gate-source capacitance and the second term is usually referred to as quantum capacitance [9]. Therefore the capacitance matrix has a rank of 3, and due to quantum capacitances the matrix is not symmetric ($C_{ij} \neq C_{ji}$). In this work we assumed that only the gate voltage changes, whereas the voltages of the other terminals are kept constant. Therefore, the capacitance matrix simplifies to three components, and an equivalent circuit as shown in Fig. 2 is achieved [16]. In Fig. 2, g_m is the differential transconductance calculated by $g_m = \partial I_{ds}/\partial V_{gs}$ Based on the equivalent circuit in Fig. 2, the cutoff frequency of the device can be derived as

$$f_T = \frac{g_m}{2\pi C_{sg}\sqrt{1 + 2\frac{C_{dg}}{C_{sg}}}} \tag{13}$$

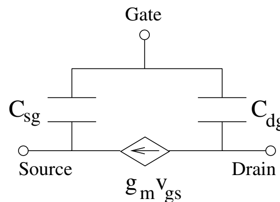

Fig. 2. Simplified equivalent circuit model for the dynamic response of CNTFETs. The model is based on the assumption that only the gate voltage changes.

3 Simulation Results

We consider a p-type ohmic device, where holes see no barrier while the barrier height for electrons is E_g. For a fair comparison with experimental results, we used the same material and geometrical parameters as reported in [5]. As shown in Fig. 3, there is a good agreement between simulation and experimental results despite the fact that the cylindrical structure is only an approximation of the real device structure.

The dynamic response of these devices has been also investigated. Fig. 4 shows the electrostatic and quantum capacitances associated with the source and drain contacts. It is clearly seen that the quantum capacitances unlike

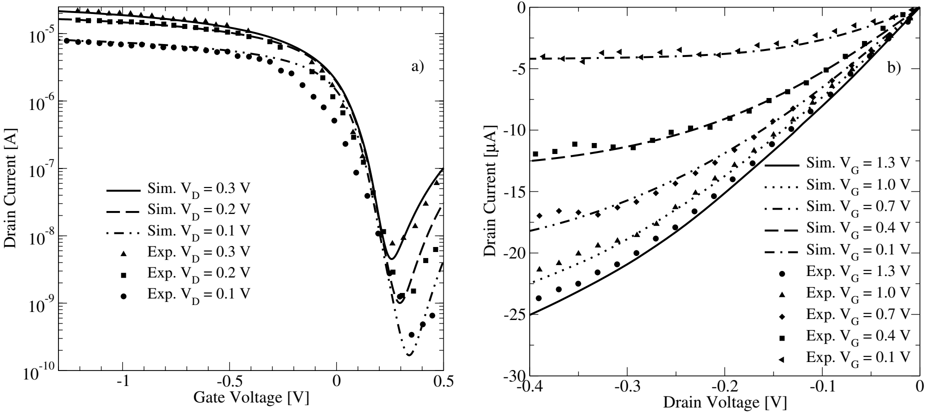

Fig. 3. The comparison of simulation and experimental results. Material and geometrical parameters are reported in [5]. a) Transfer characteristics. b) Output characteristics.

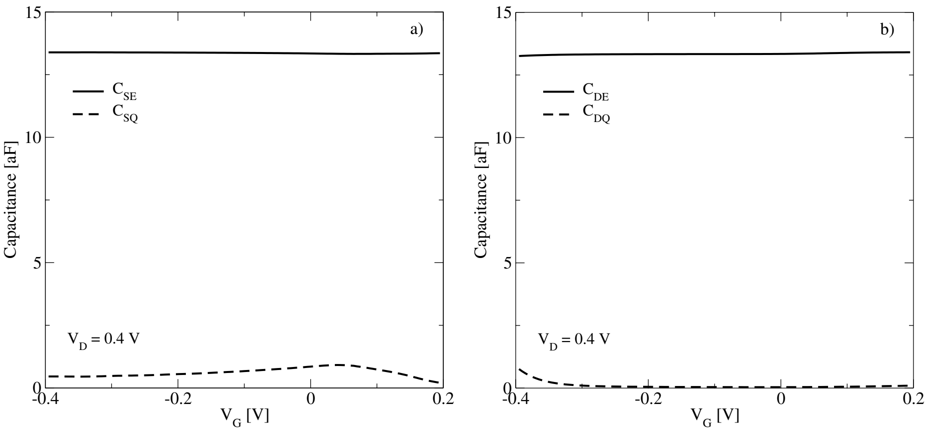

Fig. 4. Electrostatic and quantum capacitances associated with the a) Source contact, and b) Drain contact. Electrostatic capacitances dominate at low gate biases.

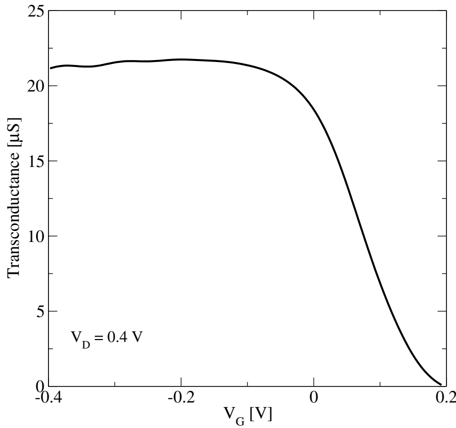

Fig. 5. The differential transconductance at different gate voltages

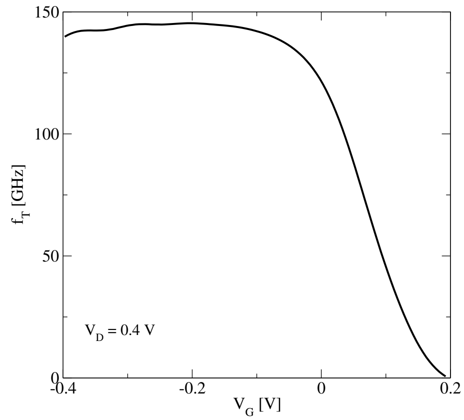

Fig. 6. Cut-off frequency at different gate voltages

the electrostatic capacitances depends on the bias voltages. At low gate voltages electrostatic capacitances dominates the quantum capacitances. To investigate the ultimate frequency limit of this device the differential transconductance of this device is shown in Fig. 5, and based on (13) the cut-off frequency is shown in Fig. 6. The cut-off frequency of the device can be improved by decreasing the parasitic capacitances, which can be achieved by increasing the source and drain spacers. However the ultimate limit will be the quantum capacitances.

4 Conclusion

We showed that by using an adaptive integration method the iterative solution of the coupled Poisson and Schrödinger equation system will converge very fast and in most of the simulations no damping is required. This method was used to study the dynamic and static behavior of CNTFETs. Good agreement between simulation and experimental results indicates the validity of the models. This methodology can be well applied for the optimization of the CNTFETs.

Acknowledgments

This work was partly supported by the European Commission, contract No. 506844 (NoE SINANO), and the National Program for Tera-level Nano-devices of the Korea Ministry of Science and Technology as one of the 21st Century Frontier Programs. Discussions with Prof. David Pulfrey are acknowledged.

References

1. Appenzeller, J., Radosavljevic, M., Knoch, J., Avouris, P.: Tunneling Versus Thermionic Emission in One-Dimensional Semiconductors. Phys.Rev.Lett. **92** (2004) 048301
2. Biegel, B.A.: Quantum Electronic Device Simulation. Dissertation, Stanford University (1997)
3. Datta, S.: Electronic Transport in Mesoscopic Systems. Cambridge University Press (1995)
4. Guo, J., Datta, S., Lundstrom, M.: A Numerical Study of Scaling Issues for Schottky Barrier Carbon Nanotube Transistors. IEEE Trans. Electron Devices **51** (2004) 172–177
5. Javey, A., Guo, J., Farmer, D.B., Wang, Q., Yenilmez, E., Gordon, R.G., Lundstrom, M., Dai, H.: Self-Aligned Ballistic Molecular Transistors and Electrically Parallel Nanotube Arrays. Nano Lett. **4** (2004) 1319–1322
6. Javey, A., Guo, J., Wang, Q., Lundstrom, M., Dai, H.: Ballistic Carbon Nanotube Field-Effect Transistors. Letters to Nature **424** (2003) 654–657
7. Javey, A., Tu, R., Farmer, D.B., Guo, J., Gordon, R.G., Dai, H.: High Performance n-Type Carbon Nanotube Field-Effect Transistors with Chemically Doped Contacts. Nano Lett. **5** (2005) 345–348
8. John, D., Castro, L., Pereira, P., Pulfrey, D.: A Schrödinger-Poisson Solver for Modeling Carbon Nanotube FETs. In: Proc. NSTI Nanotech. **3** (2004) 65–68
9. John, D.L., Castro, L.C., Pulfrey, D.L.: Quantum Capacitance in Nanoscale Device Modeling. J.Appl.Phys. **96** (2004) 5180–5184
10. Kerkhoven, T., Galick, A.T., Ravaioli, U., Arends, J.H., Saad, Y.: Efficient numerical simulation of electron states in quantum wires. J.Appl.Phys. **68** (1990) 3461–3469
11. Kim, B.M., Brintlinger, T., Cobas, E., Zheng, H., Fuhrer, M., Z.Yu, Droopad, R., Ramdani, J., Eisenbeiser, K.: High-Performance Carbon Nanotube Transistors on SrTiO3/Si Substrates. Appl.Phys.Lett. **84** (2004) 1946–1948
12. Lake, R., Klimeck, G., Bowen, R.C., Jovanovic, D., Blanks, D., Swaminathan, M.: Quantum Transport with Band-Structure and Schottky Contacts. Phys.stat.sol.(b) **204** (1997) 354–357
13. Laux, S.E.: Techniques for Small-Signal Analysis of Semiconductor Devices. IEEE Trans. Electron Devices **32** (1985) 2028–2037
14. Lin, Y.M., Appenzeller, J., Knoch, J., Avouris, P.: High-Performance Carbon Nanotube Field-Effect Transistor with Tunable Polarities. cond-mat/0501690 (2005)
15. Lyness, J.N.: Notes on the Adaptive Simpson Quadrature Routine. J.ACM **16** (1969) 483–495
16. Pulfrey, D.L., Castro, L., John, D., Pourfath, M., Gehring, A., Kosina, H.: Method for Predicting f_T for Carbon Nanotube Field-Effect Transistors. submitted to IEEE Tran. Nanotechnology (2005)
17. Radosavljevic, M., Appenzeller, J., Avouris, P., Knoch, J.: High Performance of Potassium n-Doped Carbon Nanotube Field-Effect Transistors. Appl.Phys.Lett. **84** (2004) 3693–3695
18. Rho, K.M., Lee, K., Shur, M., Fjeldly, T.A.: Unified Quasi-Static MOSFET Capacitance Model. IEEE Trans. Electron Devices **40** (1993) 131–136
19. Saito, R., Dresselhaus, G.D., Dresselhaus, M.S.: Physical Properties of Carbon Nanotubes. Imperial College Press (1998)
20. Stern, F.: Iteration Methods for Calculating Self-Consistent Fields in Semiconductor Inversion Layers. Phys.stat.sol.(b) **6** (1970) 56–67